Circular slit-groove plasmonic interferometers: a generalized approach to high-throughput biochemical sensing

Jing Feng, Dongfang Li, and Domenico Pacifici*

School of Engineering, Brown University, Providence, Rhode Island 02912, USA
**domenico_pacifici@brown.edu*

Abstract: A class of plasmonic interferometers consisting of a circular slit flanked by a concentric circular groove is demonstrated. Laying in-between the conventional bullseye and the linear slit-groove interferometers, these circular slit-groove interferometers show a polarization-insensitive optical response (thanks to the rotational symmetry imposed by the circular geometry), and overall higher light transmission (due to the absence of a cutoff condition in the circular subwavelength slit). Light transmission and sensitivity can be further enhanced by the presence of plasmonic resonant modes excited by the circular slit. The proposed circular plasmonic interferometers can be employed to develop improved biochemical sensors.

OCIS codes: (240.6680) Surface plasmons; (250.5403) Plasmonics; (260.3160) Interference; (280.4788) Optical sensing and sensors; (310.6628) Subwavelength structures, nanostructures.

References and links

1. J. N. Anker, W. P. Hall, O. Lyandres, N. C. Shah, J. Zhao, and R. P. Van Duyne, "Biosensing with plasmonic nanosensors," Nat. Mater. **7**(6), 442–453 (2008).
2. T. W. Ebbesen, H. J. Lezec, H. F. Ghaemi, T. Thio, and P. A. Wolff, "Extraordinary optical transmission through sub-wavelength hole arrays," Nature **391**(6668), 667–669 (1998).
3. H. Raether, *Surface Plasmons on Smooth and Rough Surfaces and on Gratings* (Springer-Verlag Berlin Heidelberg, 1988).
4. J. R. Krenn, A. Dereux, J. C. Weeber, E. Bourillot, Y. Lacroute, J. P. Goudonnet, G. Schider, W. Gotschy, A. Leitner, F. R. Aussenegg, and C. Girard, "Squeezing the Optical Near-Field Zone by Plasmon Coupling of Metallic Nanoparticles," Phys. Rev. Lett. **82**(12), 2590–2593 (1999).
5. A. Otto, "Excitation of nonradiative surface plasma Waves in Silver by the method of frustrated total reflection," Phys. **216**(4), 398–410 (1968).
6. E. Kretschmann and H. Raether, "Radiative decay of non radiative surface plasmons excited by light," Z. Naturforsch. B **23A**, 2135–2136 (1968).
7. D. Pacifici, H. J. Lezec, H. A. Atwater, and J. Weiner, "Quantitative determination of optical transmission through subwavelength slit arrays in Ag films: Role of surface wave interference and local coupling between adjacent slits," Phys. Rev. B **77**(11), 115411 (2008).
8. D. Pacifici, H. J. Lezec, L. A. Sweatlock, R. J. Walters, and H. A. Atwater, "Universal optical transmission features in periodic and quasiperiodic hole arrays," Opt. Express **16**(12), 9222–9238 (2008).
9. D. Pacifici, H. J. Lezec, and H. A. Atwater, "All-optical modulation by plasmonic excitation of CdSe quantum dots," Nat. Photonics **1**(7), 402–406 (2007).
10. W. L. Barnes, A. Dereux, and T. W. Ebbesen, "Surface plasmon subwavelength optics," Nature **424**(6950), 824–830 (2003).
11. K. Kurihara and K. Suzuki, "Theoretical Understanding of an Absorption-Based Surface Plasmon Resonance Sensor Based on Kretchmann's Theory," Anal. Chem. **74**(3), 696–701 (2002).
12. K. Kurihara, K. Nakamura, E. Hirayama, and K. Suzuki, "An absorption-based surface plasmon resonance sensor applied to sodium ion sensing based on an ion-selective optode membrane," Anal. Chem. **74**(24), 6323–6333 (2002).
13. S. Roh, T. Chung, and B. Lee, "Overview of the characteristics of micro- and nano-structured surface plasmon resonance sensors," Sensors (Basel) **11**(12), 1565–1588 (2011).
14. J. Homola, I. Koudelab, and S. S. Yee, "Surface plasmon resonance sensors based on diffraction gratings and prism couplers: sensitivity comparison," Sensor. Actuat, Biol. Chem. **54**(1–2), 16–24 (1999).
15. K. A. Willets and R. P. Van Duyne, "Localized surface plasmon resonance spectroscopy and sensing," Annu. Rev. Phys. Chem. **58**(1), 267–297 (2007).

#247665 Received 10 Aug 2015; revised 30 Oct 2015; accepted 30 Oct 2015; published 4 Nov 2015

16. P. Nagpal, N. C. Lindquist, S. H. Oh, and D. J. Norris, "Ultrasmooth patterned metals for plasmonics and metamaterials," Science **325**(5940), 594–597 (2009).
17. S. Aksu, A. A. Yanik, R. Adato, A. Artar, M. Huang, and H. Altug, "High-throughput nanofabrication of infrared plasmonic nanoantenna arrays for vibrational nanospectroscopy," Nano Lett. **10**(7), 2511–2518 (2010).
18. H. Im, S. H. Lee, N. J. Wittenberg, T. W. Johnson, N. C. Lindquist, P. Nagpal, D. J. Norris, and S. H. Oh, "Template-stripped smooth Ag nanohole arrays with silica shells for surface plasmon resonance biosensing," ACS Nano **5**(8), 6244–6253 (2011).
19. J. Feng, V. S. Siu, A. Roelke, V. Mehta, S. Y. Rhieu, G. T. R. Palmore, and D. Pacifici, "Nanoscale plasmonic interferometers for multispectral, high-throughput biochemical sensing," Nano Lett. **12**(2), 602–609 (2012).
20. Y. Gao, Z. Xin, B. Zeng, Q. Gan, X. Cheng, and F. J. Bartoli, "Plasmonic interferometric sensor arrays for high-performance label-free biomolecular detection," Lab Chip **13**(24), 4755–4764 (2013).
21. V. S. Siu, J. Feng, P. W. Flanigan, G. T. R. Palmore, and D. Pacifici, "A "plasmonic cuvette": dye chemistry coupled to plasmonic interferometry for glucose sensing," Nanophotonics-Berlin **3**(3), 125–140 (2014).
22. T. Thio, K. M. Pellerin, R. A. Linke, H. J. Lezec, and T. W. Ebbesen, "Enhanced light transmission through a single subwavelength aperture," Opt. Lett. **26**(24), 1972–1974 (2001).
23. H. J. Lezec, A. Degiron, E. Devaux, R. A. Linke, L. Martin-Moreno, F. J. Garcia-Vidal, and T. W. Ebbesen, "Beaming light from a subwavelength aperture," Science **297**(5582), 820–822 (2002).
24. J. A. Schuller, E. S. Barnard, W. Cai, Y. C. Jun, J. S. White, and M. L. Brongersma, "Plasmonics for extreme light concentration and manipulation," Nat. Mater. **9**(3), 193–204 (2010).
25. F. J. García-Vidal, H. J. Lezec, T. W. Ebbesen, and L. Martín-Moreno, "Multiple paths to enhance optical transmission through a single subwavelength slit," Phys. Rev. Lett. **90**(21), 213901 (2003).
26. G. Gay, O. Alloschery, B. Viaris de Lesegno, C. O'Dwyer, J. Weiner, and H. J. Lezec, "The optical response of nanostructured surfaces and the composite diffracted evanescent wave model," Nat. Phys. **2**(4), 262–267 (2006).
27. P. E. Ciddor, "Refractive index of air: new equations for the visible and near infrared," Appl. Opt. **35**(9), 1566–1573 (1996).
28. M. Daimon and A. Masumura, "Measurement of the refractive index of distilled water from the near-infrared region to the ultraviolet region," Appl. Opt. **46**(18), 3811–3820 (2007).
29. K. T. Gunay, P. W. Flanigan, P. Liu, and D. Pacifici, "Polarization dependence of light transmission through individual nanoapertures in metal films," J. Opt. Soc. Am. B **26**(24), 1972–1974 (2001).

1. Introduction

Surface plasmon polaritons (SPPs) have received significant attention for their potential to develop high sensitivity, compact, and efficient nano-biosensors [1]. Being confined at the metal surface [2–4], the SPP propagation constant can be affected by very subtle changes in the refractive index due to analytes on the metal surface. This property makes SPPs excellent candidates for the development of real-time, label-free biochemical sensing schemes.

Generally, SPPs can be excited through the use of a prism [5,6], or metal nanostructures [7–10]. Conventional surface plasmon resonance (SPR) implementations rely on the prism-based configuration [11,12]. Comparably, sensors utilizing plasmonic nanostructures employ simpler optical geometries and thus offer great potential for system miniaturization [13–15], an essential requirement for the development of fast and portable sensing devices for various biomedical applications. Several researchers have therefore channeled their efforts into the study of different structures [16–18], among which the (linear) slit-groove (SG) interferometer and the bullseye structure (consisting of a circular shallow groove flanking a subwavelength hole) have shown great promise for future applications due to high sensitivity and their potential for multiplexing [19–21].

In this paper, we propose an alternative geometry: a circular SG structure, consisting of a circular through-slit flanked by a concentric circular shallow groove. The proposed structure represents a generalized geometry, which includes the bullseye and the linear SG structures as two extreme cases [9,19–26]. Accordingly, many benefits of the two well-known structures are retained by this geometry and can be optimized by a proper choice of parameters. The outer groove acts as a broadband source of SPPs by efficiently scattering a normally-incident white light beam into propagating SPPs and redirecting them toward the central slit, where the fields of the directly incident beam and SPP waves interfere with each other, thus modulating the light intensity transmitted through the slit. Furthermore, SPPs excited by any subwavelength segment of the circular slit can also propagate toward other parts of the slit and interfere with the incident light and with the SPPs originating from the groove, to further affect light transmission. Far-field measurements of light intensity transmitted through the slit

#247665 Received 10 Aug 2015; revised 30 Oct 2015; accepted 30 Oct 2015; published 4 Nov 2015

carry detailed information about the near-field interaction between the SPPs and the dielectric material on the metal surface. Hence, circular SG plasmonic interferometers can prove to be useful for the detection of biochemical analytes and the interplay between SPPs generated by both the circular groove and slit can further enhance the device sensitivity. Preliminary results show that, compared to a linear SG plasmonic interferometer, a circular SG plasmonic interferometer can achieve 7-fold higher sensitivity. In addition, thanks to the polarization independence property due to its rotational symmetry and the larger transmission area, a circular SG plasmonic interferometer is able to make better use of the incident light intensity, an advantage over both the bullseye and the linear SG plasmonic interferometer structures. This high light throughput characteristic is crucial for the future integration of the proposed general SG interferometer into a real-time, label-free and portable sensing platform.

2. Description, fabrication and characterization of circular plasmonic interferometers

Plasmonic interferometers consisting of circular and linear slit-groove (SG) pairs were fabricated in a gold film using a combination of micro- and nano-fabrication techniques. A 4nm-thick Ti film was first deposited onto a previously cleaned quartz slide to serve as an adhesion layer, followed by e-beam deposition of a 300nm-thick Au film. Gold was chosen because (1) it can support the excitation of long-range propagating SPPs at $\lambda > 550$ nm, and (2) it offers a surface that is stable and resilient upon exposure to various chemical environments, making it a good material choice for sensing applications. Several arrays of plasmonic interferometers were then fabricated by focused ion beam (FIB) milling, using a Ga-ion beam current of ~100 pA and an accelerating voltage of 30 kV.

Figure 1(a) shows the SEM image of a representative circular SG plasmonic interferometer, consisting of a 100nm-wide circular slit entirely etched through the metal film, with radius $R_S = 2.5$ μm, and a concentric 300nm-wide, 20nm-deep circular groove, with radius $R_G = 13$ μm. The optical path in-between the slit and the groove defines the interferometer arm, with a characteristic length $p = R_G - R_S$. The sign of p is defined positive (negative) if the circular slit rests inside (outside) the area defined by the circular groove. For example, the plasmonic interferometer depicted in Fig. 1(a) has a positive arm length $p = 10.5$ μm. The bullseye and the linear SG plasmonic interferometers can be thought of as two extreme cases of the more general circular SG structure. For instance, when $R_S = 0$, the circular SG becomes a bullseye interferometer, as shown in Fig. 1(b); on the other hand, if $R_S = R_G = \infty$, the circular SG becomes a linear SG plasmonic interferometer, as shown in Fig. 1(c). Twelve columns of 246 plasmonic interferometers each were milled with various combinations of the geometric parameters mentioned above. For the circular SG case, each column has a constant R_S, while R_G varies between 0.75 and 13 μm in steps of 0.05 μm. For example, p varies from –1.75 to 10.5 μm when $R_S = 2.5$ μm. To improve the statistical significance of the experiment, two identical columns of circular SG plasmonic interferometers were milled for each R_S. The spectra of any two nominally identical devices were measured and then used to calculate a mean value at each wavelength. The procedure was repeated for each interferometer. In addition, a column of single through-slits with the same R_S was also milled to serve as the reference for normalization of the raw transmitted intensity spectra through SG plasmonic interferometers.

#247665 Received 10 Aug 2015; revised 30 Oct 2015; accepted 30 Oct 2015; published 4 Nov 2015

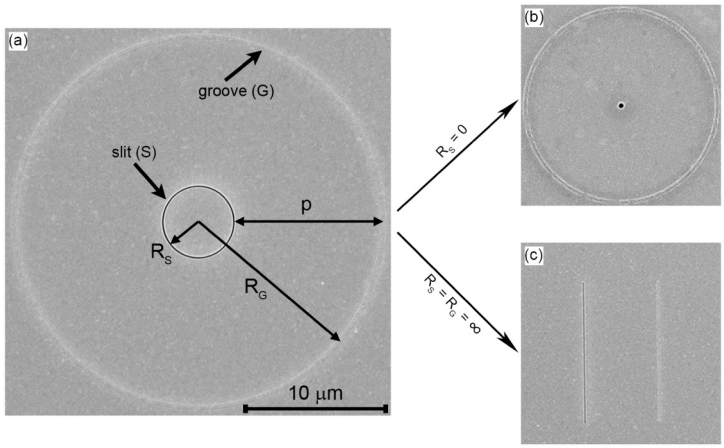

Fig. 1. (a) SEM image of a circular SG plasmonic interferometer with R_S = 2.5 μm and R_G = 13 μm. The arm length of the interferometer, defined as the separation distance between the groove and the slit, is p = 10.5 μm. The slit and groove widths are 100 and 300 nm, respectively. The depth of the groove is ~20 nm. (b) SEM image of a bullseye structure with a hole and a concentric groove, which is an extreme case of a circular SG plasmonic interferometer with R_S = 0. (c) SEM image of a linear SG plasmonic interferometer featured by a linear slit flanked by a groove, which is the other extreme case of a circular SG plasmonic interferometer with $R_S = R_G = \infty$.

The aim of this study is to determine the functional dependence of the transmitted intensity through a SG plasmonic interferometer $I_{SG}(\lambda, R_S, p)$ as a function of incident wavelength, λ, radius of curvature of the slit, R_S, as well as interferometer arm length, p. The scope of work is to experimentally identify the best configuration for sensing applications.

The intensity spectrum transmitted through the slit of each SG plasmonic interferometer was measured using a modified inverted microscope (Nikon Eclipse Ti) with automated stage, coupled to a spectrograph (Princeton Instruments Acton SpectraPro® SP-2300) and a CCD camera (Princeton Instruments PIXIS 100). A broadband light beam from a supercontinuum laser (NKT Photonics, SuperK Extreme) was collimated and focused at normal incidence onto the sample surface through the microscope condenser lens using a Köhler illumination condition with fully closed iris diaphragm. The light intensity transmitted through the slit of each plasmonic interferometer was collected by an objective lens (either 40× or 10× magnification, depending on the actual size of the circular slit) and then dispersed using the single-grating monochromator and detected by the CCD camera using a suitable region of interest. For the Au/water measurements, a polydimethylsiloxane (PDMS) microfluidic channel was used to confine and guide the flow of water onto the metal surface.

3. Optical properties of circular slit-groove plasmonic interferometers

The groove in a circular SG plasmonic interferometer works as an efficient source of propagating SPPs through diffractive scattering of the incident light beam. The circular groove focuses the SPPs in-plane and redirects them toward the inner slit where the incident beam and the SPP waves interfere, resulting in intensity modulation of the transmitted spectra through the circular slit, as a function of wavelength and interferometer arm length.

The optical properties of circular SG plasmonic interferometers, as shown in Figs. 2(a)-2(d), were characterized systematically for four specific types of circular SG plasmonic interferometers, with R_S = 0.25, 2.5, 11 μm (circular SG plasmonic interferometers) and R_S = ∞ (linear SG interferometers). For each finite value of R_S, R_G was varied between 0.75 and 13 μm, in steps of 0.05 μm. For $R_S = \infty$ (corresponding to a linear SG plasmonic interferometer), $R_G = \infty$ as well, since both the linear slit and groove have an infinite radius of curvature. The

#247665 Received 10 Aug 2015; revised 30 Oct 2015; accepted 30 Oct 2015; published 4 Nov 2015

slit and groove lengths were kept constant at 15 μm, and the SG distance p was varied between 0.25 and 8 μm. Figures 2(e)-(h) show the corresponding isolated slits. The light intensity transmitted through the slit of each plasmonic interferometer (I_{SG}) was measured and normalized to the reference light intensity transmitted through an isolated circular slit (I_S) with the same R_S, to isolate the interference effects due to SPPs propagating in between the circular slit and groove, as shown in Figs. 2(i)-(l) for representative SG plasmonic interferometers with p = 5.45 μm.

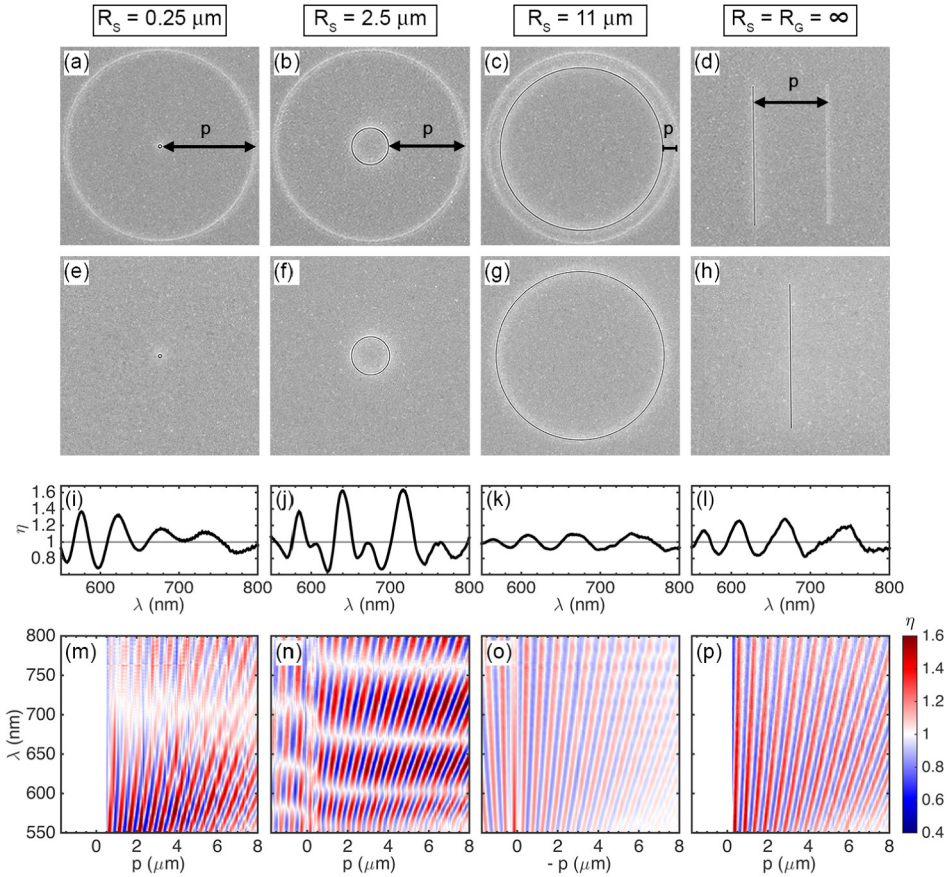

Fig. 2. (a)-(d) Representative SEM images of circular slit-groove (SG) plasmonic interferometers with different R_S: R_S = 0.25 μm (a), 2.5 μm (b), 11 μm (c), $R_S = R_G = \infty$ (d). (e)-(h) Respective SEM images of isolated circular slits with different R_S: R_S = 0.25 μm (e), 2.5 μm (f), 11 μm (g), $R_S = \infty$ (h). (i)-(l) Normalized transmitted intensity spectra for circular SG plasmonic interferometers with p = 5.45 μm, R_S = 0.25 μm (i), 2.5 μm (j), 11 μm (k), $R_S = R_G = \infty$ (l). (m)-(p) Color maps showing normalized transmission spectra (Au/air interface) for the four kinds of plasmonic interferometers, as shown above, with fixed R_S (0.25 μm, 2.5 μm, 11 μm and ∞) and varying p (–1.75 to 8 μm, in steps of 0.05 μm). For the case of R_S = 0.25 μm and the linear SG plasmonic interferometer, the experimental p value starts at 0.5 μm. In the absence of experimental data, the region p < 0.5 μm is intentionally left blank in panels (m) and (p).

A color map reporting normalized transmitted intensity defined as $\eta = I_{SG}/I_S$ can be constructed by recording and then stacking together the spectra of all the plasmonic interferometers as a function of arm length, p. A vertical cut in such a color map is the normalized transmission spectrum for a plasmonic interferometer with a specific arm length, as shown in Figs. 2(i)-2(l). Normalized intensity color maps for these four different SG

#247665 Received 10 Aug 2015; revised 30 Oct 2015; accepted 30 Oct 2015; published 4 Nov 2015

structures on an Au/air interface are displayed in Figs. 2(m)-2(p). Since R_S is different for the four configurations, even though R_G is constant, the range of p will vary accordingly. To be consistent, only spectra for interferometers with p between –1.75 and 8 μm are presented here, in order to provide for a clear comparison between the different devices. For the case of R_S = 0.25 μm as shown in Fig. 2(m), p starts at 0.5 μm. For the linear SG geometry, the spectra are symmetric for positive and negative p, assuming normal incidence for the light beam; the region with p < 0.5 μm in Figs. 2(m) and (p) has been left intentionally blank. In Fig. 2(o), since p ranges between –10.25 and 2 μm, $-p$ was adopted as the horizontal axis to show a comparable p range for all plasmonic interferometers.

Figure 2(m) presents the color map of normalized transmitted intensity obtained for the circular SG interferometer with R_S = 0.25 μm. Since the radius of the circular slit is smaller than the wavelength of the incident light (within the experimental wavelength range), the slit behaves like a subwavelength hole, and the entire circular SG plasmonic interferometer can therefore be thought of as a bullseye structure. In a single-hole/circular-groove system, it is known that the transmission through the hole can be enhanced by constructive interference of SPPs originating at the circular groove and redirected or focused toward the central hole [22–24]. It is interesting to note that the alternating oblique blue and red bands in Fig. 2(m), corresponding to suppressed (blue) and enhanced (red) light transmission respectively, are remarkably similar to the bands observed in Fig. 2(p) for a linear SG geometry with comparable arm lengths. This suggests that the periodicity observed in the normalized intensity η *vs*. arm length p at any given wavelength is dictated by SPP interference effects controlled by the changes in SPP propagative phase due to the variation in arm length, p. In simpler terms, as the distance of the groove from the slit is varied, the SPP optical path also changes, thus producing either constructive or destructive interference with the incident beam at the slit location. Also worth noting in Fig. 2(m) is the presence of a feeble yet distinct horizontal white band at around λ = 700 nm. This band neither shifts nor is modulated in intensity by a change in arm length, suggesting that its origin cannot be related to SPP waves generated by the circular groove. It is worth noting that a white pixel observed in the color map indicates a normalized transmission equal to 1, corresponding to a condition of neither enhancement nor suppression with respect to a reference single circular slit having the same diameter. The observed white band at ~700 nm can therefore be the result of the normalization procedure. For instance, at certain wavelengths, SPPs generated by the circular slit itself are so strong that the interference effect is mainly the result of the addition of the incident beam and these SPPs, and it is not affected significantly by the SPP contribution from the neighboring circular groove, which is a weaker source of electromagnetic fields. Therefore, at these specific wavelengths, the raw intensity measured through the slit of the circular SG interferometer is largely unaffected by the SPP contribution originating from the groove, leading to a value comparable to that of the isolated circular slit. Accordingly, the normalized transmission spectra will have a value of 1 at the resonant wavelength, irrespective of the interferometer arm length, p.

Figure 2(n) reports the normalized transmission intensity color map for a circular SG plasmonic interferometer with R_S = 2.5 μm as a function of incident wavelength and arm length. The radius of the slit was chosen to be 2.5 μm so that the transmission area of the circular slit and the linear slit would be similar. Besides higher normalized transmission intensity, Fig. 2(n) now shows four instead of one horizontal white bands at around 550 nm, 610 nm, 670 nm, and 765 nm for p > 0. These bands do not shift in wavelength and are not modulated in intensity when p is varied, suggesting once again that their origin is unrelated to the presence of the groove and any groove-excited SPP contribution. Observation of these bands further supports the theory that their origin is related to SPPs excited by the slit itself. Since the diameter of the cavity defined by the slit is 5 μm, more plasmonic resonant modes can be supported, compared to the previous structure with a diameter of 500 nm. Interestingly, for p < 0 the white bands experience dramatic wavelength shifts. A negative

#247665 Received 10 Aug 2015; revised 30 Oct 2015; accepted 30 Oct 2015; published 4 Nov 2015

arm length indicates that the groove is now inside the area defined by the slit, which may introduce an additional phase shift due to the presence of the groove inside the slit-defined cavity area.

Figure 2(o) shows the color map for a circular SG plasmonic interferometer consisting of a relatively large circular slit (R_S = 11 μm) and varying groove radius. For small arm lengths, i.e. when $p = R_G - R_S << R_S$, the system behaves locally like a linear SG interferometer, indeed the periodicity features observed in the corresponding color maps of the two interferometers (Figs. 2(o) and (p)) are quite similar. Due to the longer radius, the cavity defined by the slit can support more resonant modes, that are responsible for the intensity ripples observed in the color map as faint horizontal bands characterized by short oscillation periods. These bands are more visible in the top-right corner of the color map, corresponding to longer wavelengths and longer interferometer arm lengths, i.e. smaller groove radius. Incident light with longer wavelengths can be diffracted by the slit and generate SPPs that, having longer propagation lengths, can propagate across the entire cavity thus setting up weak yet observable standing wave patterns due to plasmonic resonances. Furthermore, scattering of the slit-generated SPPs by the central groove is reduced for long p, since the relatively small groove does not offer significant scattering area to the propagating SPP; therefore ripples can be observed. As p is decreased, the groove becomes a stronger scatterer for the slit-generated SPPs which reduces the strength and visibility of the horizontal ripples.

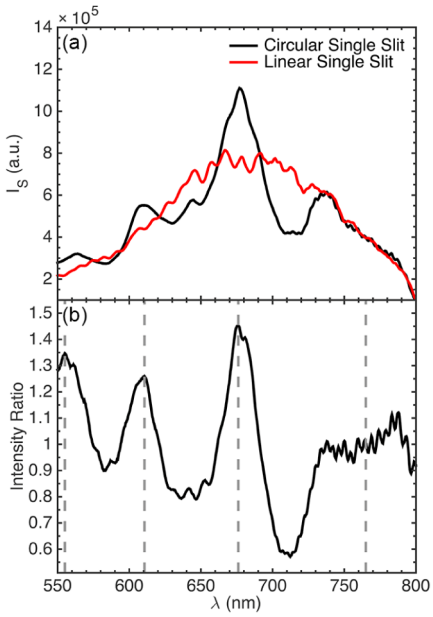

Fig. 3. (a) Raw spectra of light intensity transmitted through an isolated circular slit (R_S = 2.5 μm, black line) and a linear slit (R_S = ∞, red line). (b) Ratio between the transmitted intensity of the two structures as a function of wavelength. Four peaks are observed at ~555 nm, 610 nm, 675 nm, and 765 nm as denoted by the dashed lines, in good agreement with the horizontal white band positions observed in Fig. 2(n). Note that the reported ratio in (b) is calculated only for qualitative description and identification of the wavelength position of the resonant peaks; the specific relative intensity ratio values are therefore irrelevant since they are obtained from two totally different structures.

In order to demonstrate the hypothesis that the horizontal white bands in the color maps actually originate from the interference between the directly incident light and the SPPs excited by the circular slit rather than the groove, the transmission spectra through the isolated slits were directly measured. Figure 3(a) shows the transmission spectra through an isolated circular slit with R_S = 2.5 μm (black line) and a linear slit (red line), as well as their

#247665 Received 10 Aug 2015; revised 30 Oct 2015; accepted 30 Oct 2015; published 4 Nov 2015

intensity ratio plotted in Fig. 3(b). Four resonant peaks at ~555, 610, 675, and 765 nm are clearly observed, as denoted by the gray dashed lines, which exactly match the horizontal white band positions in Fig. 2(n). This resonant behavior can be explained by the constructive interference effect of the directly incident light and SPPs excited by the circular slit itself, which weakens the relative contribution of SPPs induced by the circular groove and results in arm-length independent white bands. However, in the region where destructive interference occurs, the SPPs excited by the groove plays a more important role in the modulation of transmitted light intensity, as confirmed by the dark blue and red regions between the white bands in Fig. 2(n), attesting to stronger interference effects.

4. Sensing experiments with slit-groove plasmonic interferometers

In this section, we compare the performance of two systems, i.e. circular SG plasmonic interferometers with R_S = 2.5 μm, and 15μm-long linear SG plasmonic interferometers. Figures 4(c)-(f) represent color maps of normalized light transmission for these two geometries (Figs. 4(a) and 4(b)) recorded in the presence of air and water, respectively. Figures 4(c) and 4(d) are the same as Figs. 2(n) and 2(p), except that a smaller p range was chosen for better comparison. Due to the refractive index change induced by water onto the gold surface, the color maps show a systematic wavelength shift and a change in the normalized intensity, clearly evidenced when comparing panel (c) with (e), and (d) with (f) in Fig. 4. Specifically, when air is replaced with water as the dielectric material in contact with the gold surface, a higher number of oscillations in normalized intensity is observed at each wavelength, due to the increased refractive index. In addition, the characteristic white bands in Figs. 4(c) and 4(e) also shift to longer wavelengths. For a straightforward comparison, representative spectra for the devices with p = 6.85 μm on Au/air and Au/water interfaces were plotted in Figs. 4(g) and 4(h), for the circular and linear geometries, respectively.

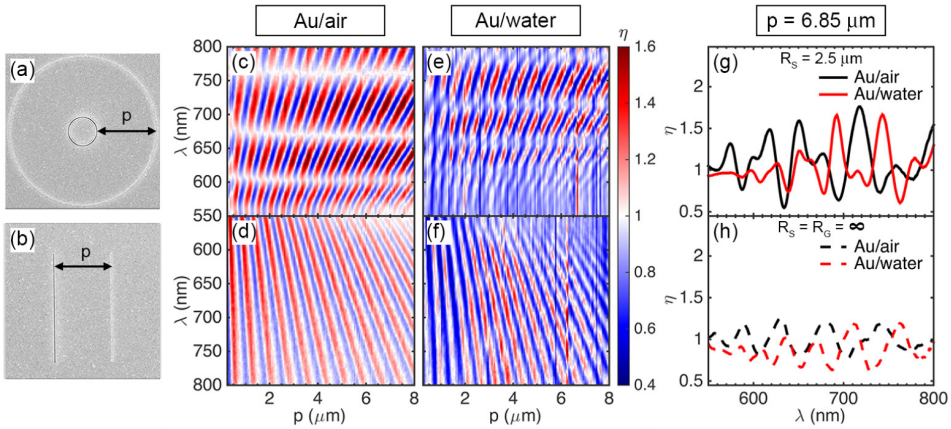

Fig. 4. (a),(b) SEM images of a representative circular (R_S = 2.5 μm) and a linear SG plasmonic interferometer. (c),(d) Color maps of normalized transmission spectra of the two types of plasmonic interferometers with varying p (0.25-8 μm, in steps of 0.05 μm) on Au/air interface. (e),(f) Color maps of normalized transmission spectra of the two types of plasmonic interferometers with varying p (0.25–8 μm, in steps of 0.05 μm) on Au/water interface. (g) Normalized transmitted spectra for a specific circular SG plasmonic interferometer (R_S = 2.5 μm, p = 6.85 μm) on Au/air (black) and Au/water (red) interfaces. (h) Normalized transmitted spectra for a specific linear SG plasmonic interferometer (p = 6.85 μm) on Au/air (black) and Au/water (red) interfaces.

Clearly, the circular SG plasmonic interferometer reaches higher normalized intensity both in air and in water. An evident advantage of the circular SG geometry is that the circular groove can focus the SPP waves toward the central slit, thus enhancing light transmission

#247665 Received 10 Aug 2015; revised 30 Oct 2015; accepted 30 Oct 2015; published 4 Nov 2015

through the slit if the arm length is chosen in such a way as to generate constructive interference. Moreover, the number of subwavelength scatterers making up the groove increases linearly with increasing groove radius, i.e. arm length p, which in turn determines a proportionally higher field amplitude at the slit location when p increases. On the other hand, as the distance between the groove and the slit is increased, the SPPs generated by each subwavelength section of the groove reach the slit with an attenuated amplitude $\sim p^{-1/2} e^{-\alpha p}$, where α is the SPP absorption coefficient due to ohmic loss in the metal. The overall net effect is that as the circular SG arm length p is increased, the total SPP amplitude at the slit location slightly increases as evidenced when looking at a horizontal cut at ~720 nm as a function of p in Fig. 4(c). This is valid only for interferometer arm lengths p such that $\alpha p << 1$, since, for $\alpha p >> 1$ the exponential decay becomes more important, causing the overall intensity to decrease as p is increased. On the contrary, the normalized transmitted intensity of the linear SG interferometer decreases monotonously as the arm length is increased, as seen from a horizontal cut at the same wavelength in Fig. 4(d). To clarify this point, Fig. 5 reports a comparison between the normalized intensities transmitted through circular and linear SG interferometers as a function of arm length, p. From Fig. 5 it is evident that the envelope function of the periodically varying normalized light intensity increases with p for circular SG interferometers, thus supporting the hypothesis provided above. The magnitude of the increase is reduced since the central slit has a finite diameter (5 μm), while the explanation provided above strictly applies to small nano-apertures placed at the center of the circular groove. In contrast, Fig. 5 also shows that the linear SG interferometer is characterized by a decreasing intensity envelope function as p increases, due to ohmic loss in the metal. Compared to the linear SG interferometer, the circular geometry can therefore mitigate the ohmic loss in the metal. The resonant cavity modes supported within the area defined by the circular slit can be tuned by simply varying the slit diameter and employed to further enhance the sensitivity of the device to small refractive index changes.

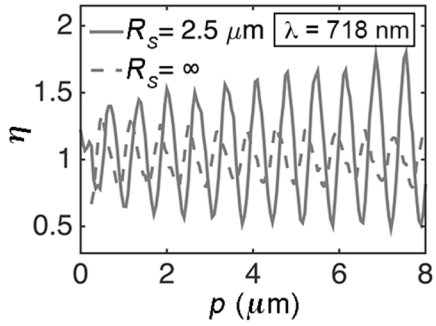

Fig. 5. Normalized light transmitted intensity measured in air through the slit of a circular SG interferometer with R_S = 2.5 μm (solid line) and through the slit of a linear SG interferometer with $R_S = \infty$ (dashed line) as a function of interferometer arm length, p, at λ = 718 nm.

To evaluate the sensing performance of each plasmonic interferometer, a figure of merit FOM_η can be defined as [19]:

$$FOM_\eta = \left| \frac{\eta_{water} - \eta_{air}}{\eta_{air}} \right| \times 100\% / \Delta n. \quad (1)$$

Here, η_{water} and η_{air} are the normalized transmitted intensities calculated when the surface of the plasmonic interferometers is in contact with water and air, respectively; $(\eta_{water} - \eta_{air})/\eta_{air}$ is a relative intensity change at a specific wavelength induced by the refractive index change Δn. Color maps of FOM_η for circular and linear SG plasmonic interferometers are shown in Figs. 6(a) and 6(b), where Eq. (1) has been evaluated taking into account the refractive index dispersion of air and water [27,28]. With specific combinations of wavelength and arm

#247665 Received 10 Aug 2015; revised 30 Oct 2015; accepted 30 Oct 2015; published 4 Nov 2015

length, the circular SG plasmonic interferometers demonstrate several times higher FOM_η than that of the linear SG plasmonic interferometers. For example, Fig. 6(c) plots FOM_η as a function of p at the wavelength of 693 nm, which corresponds to the horizontal cuts in Figs. 6(a) and 6(b). This plot is useful to determine the best device at a certain wavelength, an advantage of tunability provided by the broadband response of the subwavelength-width slit and groove in the SG plasmonic interferometers. Figure 6(d) shows the FOM_η as a function of wavelength for a specific interferometer with p = 6.85 μm. At 693 nm, the FOM_η of the circular SG plasmonic interferometer with p = 6.85 μm reaches 464%/RIU, compared with 67%/RIU for the linear plasmonic interferometer, which is a ~7 fold improvement. With optimization of the structure parameters, such as arm length, width and depth of the groove, as well as increased number of circular slits and grooves, the performance can be further enhanced. It is also important to note that the device sensitivity can be higher for smaller changes of the refractive index, as shown for example in Ref [19].

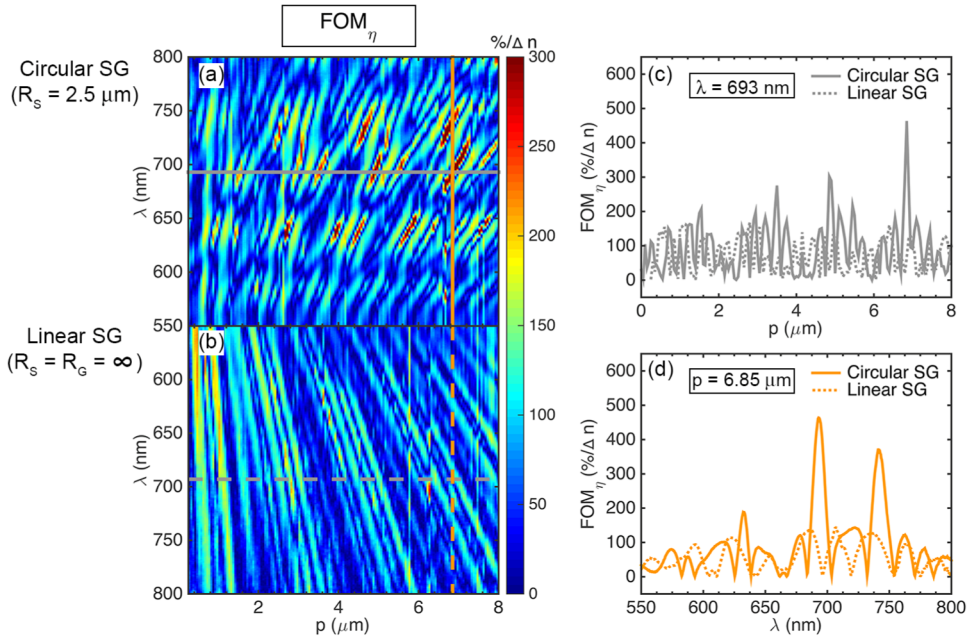

Fig. 6. (a),(b) Color maps showing FOM_η for circular (a) and linear (b) SG plasmonic interferometers with varying p (0.25–8 μm, in steps of 0.05 μm). (c) FOM_η as a function of arm length for the circular (solid line) and linear (dashed line) SG plasmonic interferometers at 693 nm, corresponding to the horizontal cuts in (a) and (b). (d) FOM_η as a function of wavelength for a circular (solid line) and a linear (dashed line) SG plasmonic interferometer with p = 6.85 μm, corresponding to the vertical cuts in (a) and (b).

It is well known that linear nano-slits on a metal film can be efficient polarizers [29]: light can be transmitted through the slits without cutoff under transverse magnetic (TM) illumination condition, i.e. when the electric field of the incident electromagnetic wave is perpendicular to the long slit axis; instead, a transverse electric (TE) incident field is highly attenuated [29]. Due to its circular symmetry, randomly polarized light can be transmitted through a circular slit without a significant loss. This property is beneficial for future integration of the interferometers onto an imaging system such as a CCD camera, which directly captures transmitted light intensity changes caused by biochemical analytes. The optical setup will be simplified without the requirement of using polarized light sources. Even though the bullseye structure is also polarization independent, due to its small aperture, the transmitted intensity is limited, compared with that through a circular SG plasmonic

#247665 Received 10 Aug 2015; revised 30 Oct 2015; accepted 30 Oct 2015; published 4 Nov 2015

interferometer, since the subwavelength hole cannot support any guided modes, and hence light transmission is cutoff for all polarizations.

To better illustrate the advantage of using a circular SG as shown in Fig. 7(a) to achieve polarization independent light transmission, a linear polarizer (Thorlabs LPVIS) with high extinction ratio (> 10^6: 1 over a broad wavelength range) was inserted into the original light path before the sample surface. The setup was also used for the measurement of light intensity transmitted through a linear SG plasmonic interferometer, as shown in Fig. 7(b). Figures 7(c) and 7(d) report the raw transmission spectra for TM (red lines) and TE (black lines) illumination conditions through representative circular and linear SG plasmonic interferometers, respectively. As shown in Fig. 7(c), a circular plasmonic interferometer shows a polarization insensitive light transmission. In contrast, the linear SG plasmonic interferometer shows more than two orders of magnitude higher transmission under TM illumination compared to TE polarization, since the linear slit is characterized by an extinction ratio > 100: 1 [29].

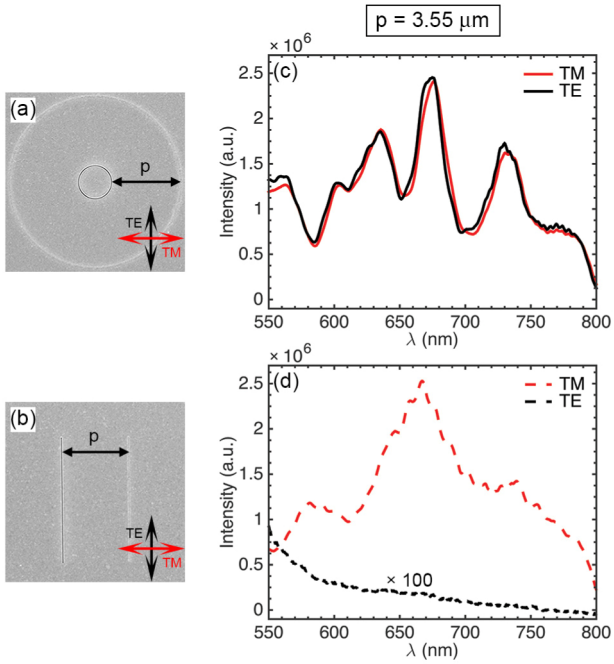

Fig. 7. (a),(b) SEM images of a representative circular (R_S = 2.5 μm) and linear SG plasmonic interferometers. The inset shows TM and TE incident polarization. (c) Raw transmitted intensity spectra for TM (red) and TE (black) polarized light through the slit of a circular SG plasmonic interferometer (with R_S = 2.5 μm, and p = 3.55 μm). (d) Raw transmitted intensity spectra for TM (red) and TE (black) polarized light measured through the slit of a linear SG plasmonic interferometer (with p = 3.55 μm). The transmitted intensity of TE-polarized light has been magnified by a factor of 100 for clarity.

Devices with high light throughput are important for potential biochemical sensors. Compared with the linear SG, the circular SG geometry can make better use of the chip area. Indeed, given a fixed device area, the length of the circular groove can be up to π times that of the linear counterpart, allowing the circular groove to couple more of the free space light intensity into SPPs. The circular slit can also be longer given the same area, and it can transmit more light. In addition, the curvature of the circular groove and slit also reduces the crosstalk between adjacent devices, which enhances the integration capability of the circular geometry for high-density, high-throughput sensing applications.

#247665 Received 10 Aug 2015; revised 30 Oct 2015; accepted 30 Oct 2015; published 4 Nov 2015

5. Conclusion

In conclusion, we reported a detailed experimental study about the design, fabrication and characterization of circular slit-groove (SG) plasmonic interferometers. These interferometers, consisting of a circular through-slit flanked by a concentric shallow groove, can be thought of as a generalization of two well-established geometries, i.e. the bullseye and the linear SG interferometers. Being characterized by an increased light transmission per unit area and a polarization-independent response, the proposed circular SG plasmonic interferometers show a significant advantage over both the bullseye and the linear SG geometries. The transmission properties of various circular SG plasmonic interferometers were studied in detail as a function of slit and groove diameters, as well as slit-groove separation distance, which defines the characteristic interferometer arm length. A circular SG plasmonic interferometer works by employing the circular groove as an efficient source of SPPs. The generated SPPs are then focused toward the central slit location, where the incident beam and the SPP contributions interfere with each other thus generating either constructive or destructive interference. Tuning of the interference conditions can be achieved by simply varying the arm length, the wavelength of the incident light, or even the slit radius. Indeed, the circular slit can also serve as an additional source of SPP resonant modes that can further modulate the transmitted intensity, a capability missing in both linear SG and bullseye plasmonic interferometers. We then assessed the potential of this class of interferometers to perform as sensors and measured their optical response upon variation of the dielectric material on top of the metal surface. Thanks to the synergistic interaction between resonant SPP modes and plasmonic interference effects, the circular SG interferometers show improved sensitivity compared to their linear counterpart. For instance, compared to the linear SG plasmonic interferometer with same arm length, the circular SG structure shows a 7-time increase in the sensitivity to refractive index change. Moreover, compared to both the bullseye and the linear slit-groove geometries, circular SG plasmonic interferometers show overall increased light transmission per unit area, thus allowing for a higher signal-to-noise ratio when coupled to an integrated photodetector. In addition, a reduced crosstalk between adjacent circular interferometers due to the circular geometry can allow for higher degrees of device integration, with achievable densities up to one million of plasmonic interferometers per square centimeter. In conclusion, the proposed circular SG plasmonic interferometers hold great promise for the realization of compact, sensitive and high-throughput platforms for various point-of-care sensing applications, such as glucose management for diabetic patients [21], or detection of relevant biomarkers.

Acknowledgments

The authors gratefully acknowledge funding from the National Science Foundation (NSF) Grant No. CBET-1159255.

#247665 Received 10 Aug 2015; revised 30 Oct 2015; accepted 30 Oct 2015; published 4 Nov 2015
